Materials & Design 208 (2021) 109902

Contents lists available at ScienceDirect

Materials & Design

journal homepage: www.elsevier.com/locate/matdes

Integrated molecular dynamics and experimental approach to characterize low-free-energy perfluoro-decyl-acrylate (PFDA) coated silicon

Annalisa Cardellini [a], Francesco Maria Bellussi [a], Edoardo Rossi [b], Lorenzo Chiavarini [a], Claude Becker [c], David Cant [d], Pietro Asinari [a,e,*], Marco Sebastiani [b,*]

[a] Politecnico di Torino, DENERG, Corso Duca degli Abruzzi 24, Torino 10129, Italy
[b] Università degli studi Roma Tre, Engineering Department, Via della Vasca Navale 79, Roma 00146, Italy
[c] Molecular Plasma Group, Technoport Hall 4B, Rue du Commerce, L-3895 Foetz, Luxembourg
[d] National Physical Laboratory (NPL), Hampton Road, Teddington TW11 0LW, UK
[e] INRiM – Istituto Nazionale di Ricerca Metrologica, Strada delle Cacce 91, Torino 10135, Italy

HIGHLIGHTS

- Integrating molecular modelling and experiments for the optimal surface characterization.
- Decoupling surface chemistry and topography contributions to address a more rational design of low-free-energy surfaces.
- Increasing the hydrophobicity of perfluoro decyl acrylate coated silicon.
- Improving the design of low-free-energy surfaces.

GRAPHICAL ABSTRACT

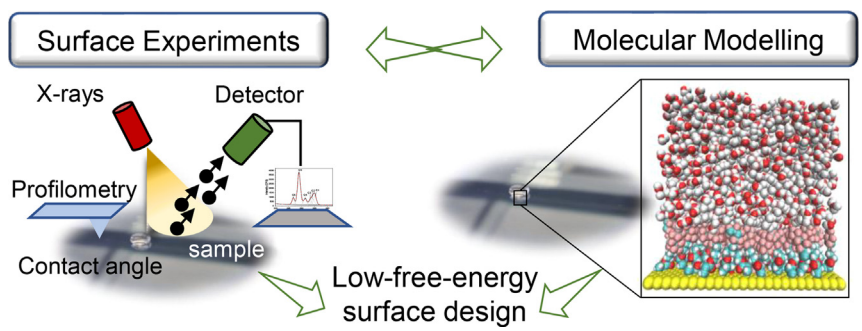

ARTICLE INFO

Article history:
Received 1 April 2021
Revised 26 May 2021
Accepted 12 June 2021
Available online 15 June 2021

Keywords:
Low-free-energy surface design
Surface characterization
Molecular dynamics
Contact angle
XPS

ABSTRACT

Low-free-energy surfaces have attracted an intense academic and industrial interest over the last decade. A reduction of the surface free energy (SFE) has been found to enhance self-cleaning, hydrophobic, and non-fouling properties of surfaces, which are highly desirable in many industrial applications. However, tuning the surface chemistry and topography to achieve tailored low free energy surfaces has been found extremely challenging. In this work, we first show that an accurate refinement of the atmospheric plasma technique guarantees a polymeric coating near to the super-hydrophobic regime. Second, by coupling modelling and experimental measurements we suggest a reliable workflow for the surface characterization and smart design. Specifically, the case study proposed in this contest is capable of quantitatively distinguishing the contribution of a Perfluoro Decyl Acrylate (PFDA) coating, and hence decoupling the role of surface chemistry and roughness, in the reduction of the surface free energy of a bare silicon sample. Beyond the specific case study, our results also emphasize that a synergistic combination of models and experiments can unveil the optimal pathway for designing low-free-energy surfaces.
© 2021 The Authors. Published by Elsevier Ltd. This is an open access article under the CC BY-NC-ND license (http://creativecommons.org/licenses/by-nc-nd/4.0/).

* Corresponding authors at: Politecnico di Torino, DENERG, Corso Duca degli Abruzzi 24, Torino 10129, Torino, Italy (P. Asinari).
E-mail addresses: pietro.asinari@polito.it (P. Asinari), marco.sebastiani@uniroma3.it (M. Sebastiani).

https://doi.org/10.1016/j.matdes.2021.109902
0264-1275/© 2021 The Authors. Published by Elsevier Ltd.
This is an open access article under the CC BY-NC-ND license (http://creativecommons.org/licenses/by-nc-nd/4.0/).

1. Introduction

The development of low-free-energy (LFE) surfaces represents one of the most attractive challenges in material science. Over the last two decades, low-free-energy surfaces and superhydrophobic materials have attracted the attention of the academics with a constant increase in research activities [1]. The interest in their development is justified by the wide range of possible industrial applications, involving several engineering fields. In general, LFE surfaces exhibit characteristics of low wettability, and therefore, anticorrosion, anti-icing, antifogging and self-cleaning properties making them widely used in mechanical, aerospace and energy applications [2–4]. Furthermore, due to their ability to repel fluids, LFE bio-compatible materials are largely employed in biomedical applications [5].

The preparation of LFE surfaces is either based on the deposition of coating films or on the creation of surface microstructures. The former involves chemical modifications, while the latter is centered on the morphological characteristics of the surface. Then, by combining the two approaches and taking advantage of the surface roughness, it is possible to generate superhydrophobic surfaces. Although the concrete technological progresses have largely improved the manufacturing protocols of LFE surfaces, this field is still lacking of specific guidelines to directly relate the characterization of surfaces with their tailored and smart design.

From an experimental point of view, there are several tools for surface energy characterization either based on contact mechanics, such as nanoindentation and atomic force microscopy (AFM), or based on wetting methods. Contact mechanics approaches are widely used for the study of bulk properties (hardness and elastic modulus), and have only recently been applied for the evaluation of the work of adhesion between sample and indenter and surface free energy (SFE) from the pull-out force [6–8]. Although promising, the contact mechanics methods require some improvements mainly related to the post-processing of the resulting SFE measurements. On the other hand, the standard approach for characterizing LFE surfaces is the static contact angle (CA) analysis, applied both for hard and soft matter [9–12]. For planar and smooth surfaces, the value of the CA is related to the surface free energy through a combination of Young's equation [13], and the Owens-Wendt method [14] based on the main hypothesis that the surface free energy is made up of two components: dispersion, (γ_S^D), and polar (γ_S^P). However, the experimental characterization is not uniquely sufficient to suggest guidelines for the optimal design of LFE surfaces. In fact, the isolated measurements of contact angles and surface energy do not provide the essential indicators to distinguish the chemical and topographical contributions to the interfacial properties, preventing the process of optimal surface design. As a consequence, the experimental characterization approaches should be coupled and integrated with tailored modelling techniques in surface science to address a smarter design. For example, when the effects of surface roughness are not negligible, the relation between the Young's CA and apparent CA could be computed by introducing the Wenzel and the Cassie-Baxter models [15,16], also coupled in following equation [17]:

$$\cos\theta_a = rf\cos\theta_Y + f - 1 \quad (1)$$

where r is the ratio between the effective contact surface and the projected surface and f represents the fraction of solid–liquid interface. This method directly provides the value of the apparent CA between the surface and the liquid droplet, considering both the chemistry and the morphological effects. Using this method, Zeng et al. and Karaman et al. [18,19] evaluate the surface wettability at different chemical compositions of PFDA polymer, demonstrating an increment of hydrophobic properties with the fluorine content, while Coclite et al. [20] studied the effect of grafting PFDA molecules to the sample surface, which induces higher values of surface roughness. Giljean et al. [21] studied the influence of surface roughness and cleaning processes on apparent CA, applying the two liquids method. In general, these works are supported by preliminary spectroscopy analysis to evaluate the surface chemical composition [18–20,22,23] and microscopic or profilometric analysis to explore the surface roughness [21,24].

From a modelling standpoint, also Molecular Dynamics (MD) simulations have been used extensively to investigate the role of water at solid–liquid interface [25–28] and specifically the wetting properties of different fluids on several surfaces [29–31]. In fact, the MD simulations provide insight about the relationship between the atomic scale features of the surface and its interface thermodynamics, helping the chemical design of materials for a wide range of applications. Specifically, both the droplet and the free energy perturbation (FEP) methods [32] have started to be used to determine the wetting properties of solid–liquid interfaces. Despite the FEP method being slightly more complex, it is believed to be more accurate [33,34]. As pointed out by Leroy, the work of adhesion is more reproducible than the contact angle, allowing a safer evaluation of the wetting properties or force field derivation [33]. In fact, the water contact angle has been found to be strongly dependent on the water model chosen in the droplet methods. This is due to the fact that no model is able to perfectly reproduce the experimental surface tension of water: variation among the most popular models can be as large as 10–15%. On the other hand, the FEP approach is based on small perturbations of the interaction potential parameters at the interfaces without changing their atomic coordinates from the unperturbed system [31].

Besides the strong efforts made to fully characterize the low-free-energy surfaces, many challenges still remain unsolved. CA measurements require sufficiently planar surfaces to be reproducible and their value could be strongly affected by the presence of contaminants [35]. Moreover, as already mentioned, the use of a single technique, either experimental or modelling may underestimate key parameters which control the interfacial behavior, thereby restricting the variety of designing elements to play with. In addition, merely the validation criteria, mainly applied to connect models and experiments, may also give inappropriate results if erroneous space-scale phenomena are considered when comparing the results. For example, a macroscopic characterization tool like contact angle, although accurate and reliable in the measurements and analysis, reveals strong limitations to differentiate between nanoscale design parameters, surface chemical contaminants, and roughness which all influence the interfacial properties. Moreover, the molecular models used to compare the experimental results are often based on a theoretical composition of the considered sample, thus they may differentiate and be less representative of the real and specific material used for the measurements. For this reason, diverse characterization approaches have to be synergistically integrated and coupled to precisely describe the sample and characterize its wetting behavior giving specific suggestions for an optimal rational design of low-free-energy surfaces.

In this article, with aim of providing possible guidelines for a more rational design, we propose a coupled experimental and modelling approach able to improve the quality of the low-free energy surface characterization and to address the manufacturing protocols. In detail, a semi-dynamic Dielectric Barrier Discharge (DBD) plasma has been tailored to fabricate (1H,1H,2H,2H)-Perfluorodecyl acrylate (PFDA) coated silicon surface, demonstrat-

ing high efficacy in obtaining a hydrophobic surface [36–38]. Extensive experimental studies have already demonstrated the insolubility of such polymers in the most common solvents, mostly due to the fluorine groups CFx [18,19]. Therefore, PFDA polymer has been widely used because of its capability to create aggregated lamellar structures that enhance hydrophobicity, while still remaining bio-and eco-compatible. The chemical analysis obtained from X-ray photoelectron spectroscopy (XPS) and the contact angle measurements have provided the quantitative information about PFDA coated surface properties. Beyond the wettability characterization, these experimental results have allowed to define and to build up a reliable and chemically consistent MD model, which unveils the role of chemistry on the contact angle experimental measurements thereby addressing a more tailored material design. The results show that the atmospheric plasma polymerization method, tuned and refined in this context to fabricate polymer coated silicon, guarantees the production of low-free-energy surfaces near to the super-hydrophobic regime, as highlighted by the experimental contact angle results. Moreover, the integration of XPS and CA measurements with molecular modelling and profilometric analysis, defines a clear design framework to guide the industrial production of surface coatings.

2. Material and methods

2.1. Sample preparation

A semi-dynamic Dielectric Barrier Discharge (DBD) plasma system has been used at atmospheric pressure and open-air conditions. In comparison to vacuum plasma techniques, the atmospheric set-up has numerous advantages such as, low-cost equipment, large samples, complex shapes treatments, high deposition rates, the possibility of using numerous gases and precursors, which finally facilitate technology transfer according to industrial requirements. The most advanced atmospheric techniques show remarkable control in the deposition parameters leading to a high retention of monomer functionalities and a stable polymerization close to conventional methods. Coatings produced using these new processes evidenced a perfect homogeneity, high mechanical and optical properties, and excellent thermal and chemical stabilities [36–38]. The plasma discharge was produced between an earthed aluminum electrode and two high voltage aluminum plates separated by a dielectric (boro-silicate glass). The gap between both electrodes was set to 2 mm and the plasma discharge surface was 300 cm^2. In a first process step, the DBD plasma reactor was used using only nitrogen in order to clean and to activate the silicon substrates purchased from Siegert wafer GmbH. Then the precursor monomer was introduced as nano-sized droplets in the plasma discharge by using an atomizer system (from TSI corp. Company) with a flow rate of 3 SLM by using nitrogen gas to atomize the chemical precursor and to generate the plasma discharge, using an AC power supply from AFS/SOFTAL. The precursor monomer (1H,1H,2H,2H-perfluorodecylacrylate), purchased from conventional chemical products providers companies, was used as received. The thickness of the coatings achieved are related to the deposition duration and the growth rates depend on the plasma deposition conditions (gas, power, frequency, gap between both electrodes and the monomer flow rate). A schematic representation of the DBD plasma set up is illustrated in Fig. 1.

3. Experimental characterization

3.1. XPS measurements

XPS analysis of the sample was performed using a Kratos Axis Ultra instrument in 'hybrid' mode using a monochromated Al Kα x-ray source (photon energy 1486.6 eV) operating at 5 mA emission current and 15 kV anode voltage. Survey spectra were obtained from the sample at a pass energy of 160 eV, and higher resolution spectra for the carbon 1s peaks were taken at a pass energy of 20 eV. In order to mitigate the effects of sample charging under the X-ray beam, a low-energy electron flood gun was used. The energy scale was then referenced to the hydrocarbon component of the C 1s peak at 285 eV binding energy. Determination of the equivalent homogeneous atomic composition was performed from the survey spectra using Casa XPS software, version 2.3.22. The intensity scale of the spectra was corrected using the NPL transmission function [39], and the NPL average-matrix relative

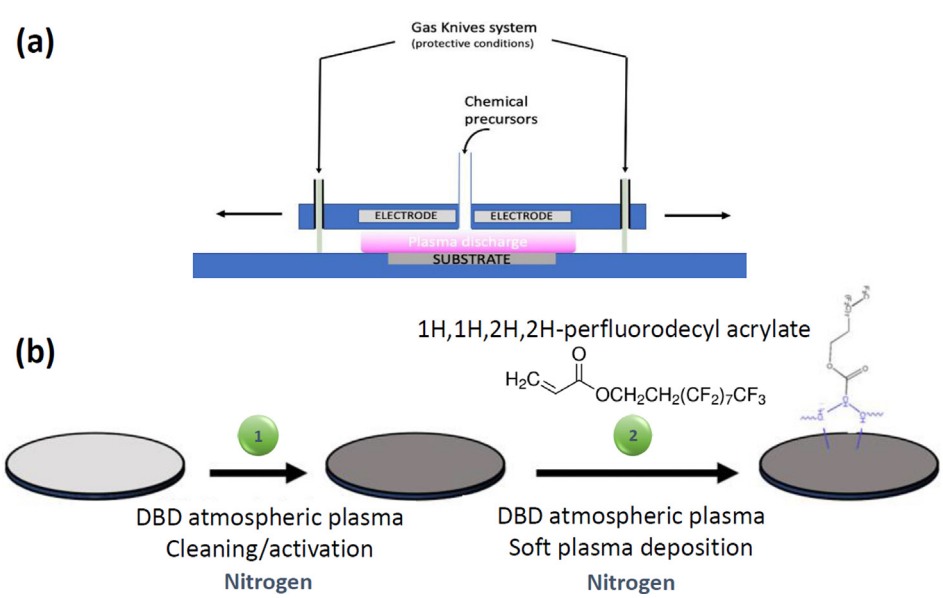

Fig. 1. (a) Schematic illustration of the semi-dynamic Dielectric Barrier Discharge (DBD) plasma system. (b) Description of the two stages employed to prepare the PFDA coated silicon wafer using the DBD atmospheric plasma: (1) cleaning/activiatation, and (2) soft plasma deposition.

sensitivity factors (AMRSF's) were applied to peak areas determined after application of a Tougaard background (ISO 18118:2015) [40].

3.2. Contact angle measurements

The contact angle measurements were accomplished using a contact angle meter equipment realized at Roma Tre University, respecting the relative normative standards (UNI EN 828, UNI 9752, ASTM D-5725-99) (see Fig. S.2 in the SI document). Three different reference liquids were used: water, formamide (polar liquid), and methylene iodide (nonpolar liquid). For each liquid, six drops (with volumes of 3 μl) were deposited on the sample's surface. The environment boundary conditions were room temperature (20–22 °C) and humidity between 25% and 35%. The sessile drop technique was used: the images of the liquid drops were captured by Olympus Soft Imaging System and successively elaborated by Analysis Image software to improve the accuracy of the contact angle measurements (see Fig. 3 (a)). The contact angle measurements were coupled with the application of the analytical Owens-Wendt method [14,41–43], since it represents one of the most used and validated methods for the surface energy calculation [42,44]; the main hypothesis of this model is that the surface free energy is made up of two components: dispersion, (γ_S^D), and polar (γ_S^P) components. The geometric mean relationship is:

$$\frac{1}{2}(1+\cos\theta)\cdot\gamma_l = (\gamma_S^D\cdot\gamma_l^D)^{\frac{1}{2}} + (\gamma_S^P\cdot\gamma_l^P)^{\frac{1}{2}} \quad (2)$$

where θ is the contact angle value between the surface and the liquid drop, $\gamma_l$is the liquid surface tension, γ_S^D, and γ_l^D are the dispersion component of the solid and liquid surface tension, respectively, while γ_S^P and γ_l^P are the polar components of the solid and liquid surface free energy. The dispersion and polar components of the solid surface free energy are the unknown variables. The value of total surface free energy of the solid is obtained using the following equation:

$$\gamma_S = \gamma_S^D + \gamma_S^P \quad (3)$$

The geometric mean relationship could be written also as:

$$\frac{(1/2)(1+\cos\theta)\gamma_l}{(\gamma_l^P)^{1/2}} = \left(\frac{\gamma_l^D}{\gamma_l^P}\right)^{1/2}\cdot(\gamma_S^D)^{\frac{1}{2}} + (\gamma_S^P)^{\frac{1}{2}} \quad (4)$$

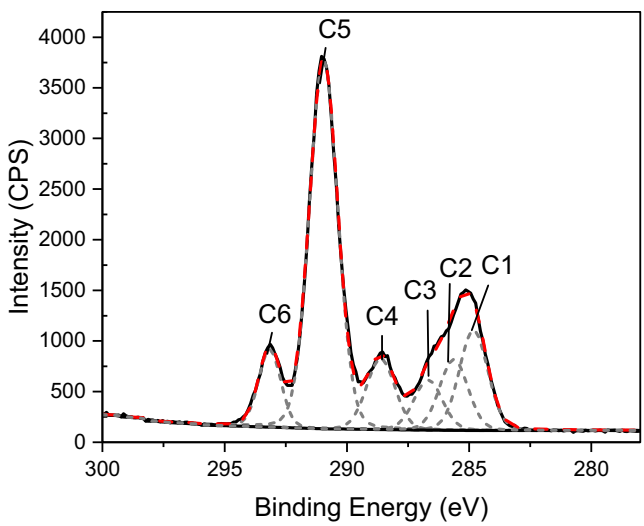

Fig. 2. Example fit of a carbon 1 s spectrum; the peak fit is indicated with dashed lines, and each component is labelled.

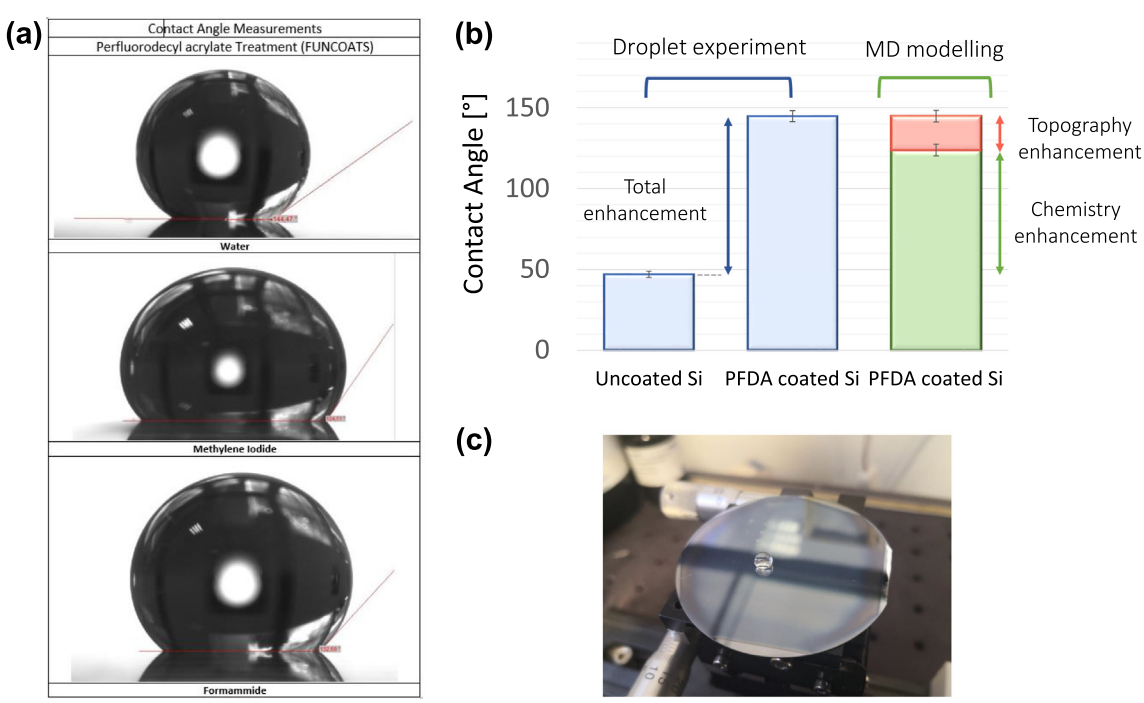

Fig. 3. (a) Droplet of water (top), methylene Iodide (center) and formammide (bottom) on the PFDA coated silicon sample. (b) Estimation of the Contact Angles (CA) obtained both with the droplet experimental measurements on Uncoated and PFDA coated Silicon (light blue bars) and with Molecular Dynamics (MD) model after following the FEP approach (green bar). Note that the MD CA is 123.8° ± 3.6°, obtained as an average value in the configuration window between iii and iv (see Fig. 5). The MD model is able to distinguish the chemical contribution to the total CA enhancement obtained from the PFDA coating. Profilometric analysis confirms instead the topography enhancement of CA. (c) Water droplet on top of the PFDA coated sample. (For interpretation of the references to color in this figure legend, the reader is referred to the web version of this article.)

where on the left there are quantities measured by experiments (θ) or known from literature (γ_l^P and γ_l) [45–47], so that a plot of the left-hand quantities versus $\left(\frac{\gamma_l^D}{\gamma_l^P}\right)^{1/2}$ gives a straight line with slope $(\gamma_S^D)^{\frac{1}{2}}$ and intercept $(\gamma_S^P)^{\frac{1}{2}}$.

3.3. Profilometric analysis

The profilometric analysis were performed by a Leica DCM 3D profilometer according to ISO 25178 and ISO 4287 standards to obtain the roughness values (Table 4) on three different regions of the sample and applying a Gaussian filter with a cut-off value of 25 μm (Tables S1 and S2). The acquisitions were performed in confocal mode using a 100x optical object with blue light.

3.4. Modelling characterization: Molecular dynamics (MD) simulations

The MD configurations, adopted to compute the work of adhesion with the FEP approach [32], are characterized by a film of water of approximately 10 nm thickness in contact with a lower layer of 140 PFDA molecules distributed in a surface of 6.42x6.42 nm^2. Fig. 4(a) show the PFDA-water configuration arranged for the FEP simulations. We point out that differently from the droplet method, in which the results are sensitive to the droplet dimension, requiring a polymer surface area sufficiently large to avoid possible interactions between the droplet itself and its periodic image, the FEP approach explores the interface in the bulk region, making the simulation insensitive to border effects in x and y direction. The initial coordinates of a single PFDA molecule were obtained in Open Babel [48]. With the aim to reproduce the ordered PFDA coating observed experimentally from the atmospheric plasma polymerization [36], we packed the polymer molecules perpendicularly to the PFDA-water layering as illustrated in Fig. 4(a). In addition, to preserve the strong structured configurations, a wall potential was applied from the bottom wall of the simulation domain with a strong LJ interaction with the designed atom of the polymer chain. In line with the XPS results, 4 distinct atomistic configurations were created by modifying the CF_x orientation, namely:

i. 0% of CF_x groups in contact with water (Fig. 5 (a1)),
ii. 60% of surface CF_x in contact with water (Fig. 5 (a2)),
iii. 80% of surface CF_x in contact with water (Fig. 5 (a3)),
iv. 100% of surface CF_x, perfectly orientated and exposed to water (Fig. 5 (a4)).

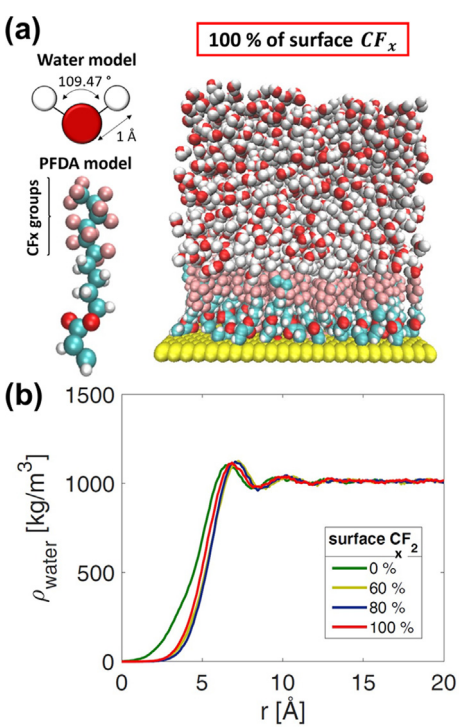

Fig. 4. (a) Left: Molecular Dynamics (MD) model of SPC/E water and PFDA molecules. Right: MD snapshot of water-PFDA interface at 100% of surface CF_x. (b) Water density profiles from the uppermost PFDA coating (r = 0 Å) for different CF_x orientation. Color code: oxygen atoms are in red, hydrogen atoms are in white, carbon atoms are in cyan, fluorine atoms are in pink and the basement wall in yellow. (For interpretation of the references to color in this figure legend, the reader is referred to the web version of this article.)

Periodic boundary conditions were employed in the two interface planar dimensions (x and y). On the other hand, fixed boundary conditions were used in the direction perpendicular to the interface (z) applying the slab correction for the long-range electrostatic interactions, to avoid any possible interaction with the periodic image [65]. The topology files corresponding to the initial set-up previously described were generated in GROMACS [49], where the OPLS-AA force field [50], particularly suitable to model soft matter in water, was implemented to model both the PFDA and the SPC/E water molecules. The effectiveness of OPLS-AA with respect to other soft matter force fields is also demonstrated by D. Shivakumar et al. who computed the solvation free energy using the FEP approach [51]. On the other hand, the main advantage of the SPC/E model consists of reproducing some macroscopic properties of water with good accuracy, still maintaining a limited computational time during the simulated dynamics. As example, a comparison of surface tensions obtained with SPC/E, Tip3P, Tip4P, and Tip5P water models is reported in Fig. S.3 in the SI document [52]. Gro2LAM tool [53] was employed to convert the GROMACS input files to the open source LAMMPS [54] data types. The MD simulations were finally performed using the open source LAMMPS software. The complete set of molecular topology, including the initial configurations and simulation input data are collected in the SI documentation. The electrostatic interactions were calculated using the particle–particle particle-mesh approach to the Ewald summation as implemented in LAMMPS. Both the electrostatic interactions in the real space and the Lennard-Jones interactions were calculated with a cutoff distance of 1 nm. A time step of 1 fs was employed to integrate the equations of motion.

The four atomistic configurations listed before (i–iv), were considered to calculate the work of adhesion, W_{sl}, at PFDA-water interface by implementing the FEP approach [32], namely:

$$W_{sl} = \frac{1}{A}\sum_{i=0}^{n-1}\Delta_{\lambda_i}^{\lambda_{i+1}}G = -kT\sum_{i=0}^{n-1}\ln\left\langle \exp\left(-\frac{U(\lambda_{i+1})-U(\lambda_i)}{kT}\right)\right\rangle_i \quad (5)$$

where k is the Boltzmann constant, T the temperature, U the interaction energy between PFDA and water molecules, ΔG is the free energy change, and λ is the coupling parameter employed to gradually reduce the Lennard-Jones attraction and the Coulombic forces to zero. After the energy minimization, the simulations were equilibrated for 2 ns in the NVT ensemble, keeping the temperature constant at 293.15 K with a Nose-Hoover thermostat [55] whose damping parameter was set to 100 fs. Then, coherently with the FEP protocol, for each atomistic configuration (1–4), 20 independent MD runs were carried out by tuning the soft-core interaction energy with lambda parameter ranging from 1 to 0 with a step of 0.05. The total production runs were carried out in NVT ensemble for 8 ns. The perturbated potential energies U obtained were collected to compute the Boltzmann factor and consequentially the work of adhesion, W_{sl}, as shown in Eq. (5). Note that the Boltzmann

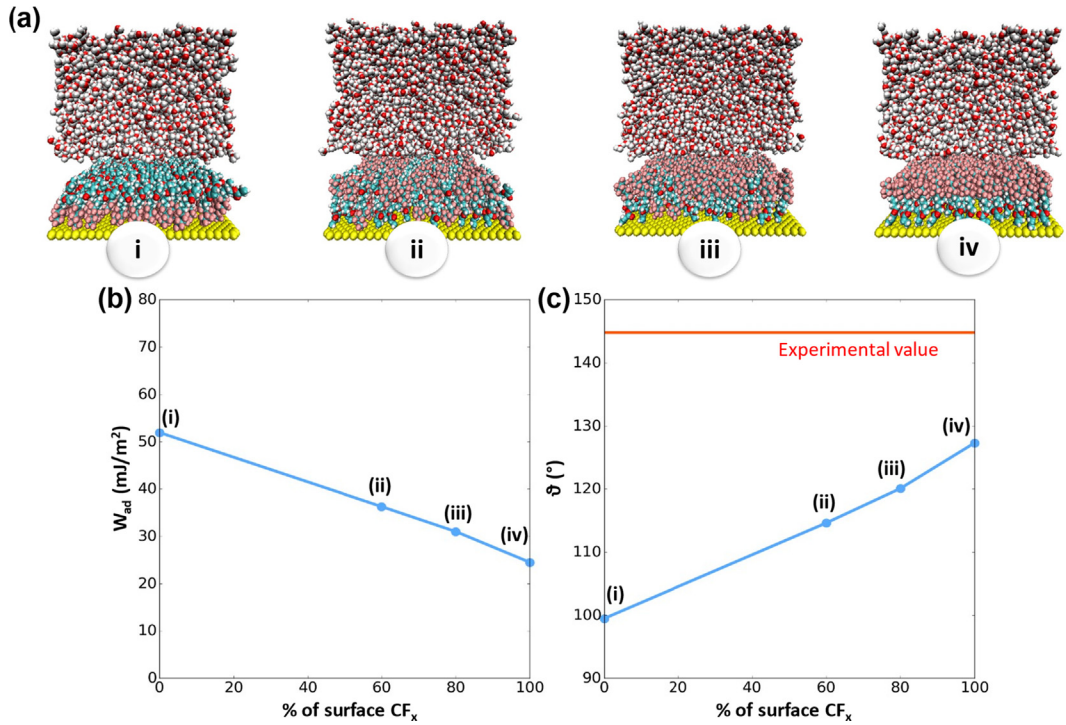

Fig. 5. (a) MD snapshot of water-PFDA interfaces with 0% (i), 60% (ii), 80% (iii) and 100% (iv) of CFx groups in contact with water. Note that the nearest layer of water molecules to the PFDA atoms has been removed for clarity purpose, thereby uncovering the uppermost surface of the polymer coating. (b) Work of adhesion, *Wsl*, at PFDA-water interface corresponding to the four configurations depicted in (a). W_{sl} is computed by implementing the FEP approach described in the Equation (5). (c) Estimation of the contact angles obtained by coupling the W_{sl} in (b) with the Young-Dupré in equation (6). Note that, the results show a variation less than 0.1 mJ/m^2 and equal to 1° on the W_{sl} and contact angle, respectively (see the Method section for more details).

factor corresponds to the exponential term into the ensemble average brackets in the equation (5). Finally, W_{sl} was included into the Young-Dupré equation to estimate the contact angles, ϑ, of water on the modelled PFDA coating, namely [56]:

$$W_{sl} = \gamma_{LV}(1 + cos\theta) \tag{6}$$

where γ_{LV} is the surface tension of spc/e model of water, namely 62.34 ± 1.43 mJ/m^2, calculated applying the Irvine-Kirkwood relation [52]. The error bars on the resulting W_{sl} and contact angle were calculated using at least three different initial MD configurations, for each FEP calculation, obtained by varying the canonical ensemble during the equilibration steps. The results show a variation less than 0.1 mJ/m^2 and equal to 1° on the W_{sl} and contact angle, respectively.

4. Results and discussion

The characterization framework proposed in this article includes experimental and modelling techniques to both improve the understanding of surface properties and to address a more rational design of coated surfaces. First, the experimental results of XPS and contact angle (CA) measurements clarify the surface chemistry composition and the wettability properties, respectively, of PFDA coated silicon sample. Then, a consistent molecular modelling is proposed to quantitatively decouple the role of chemistry and roughness on the interfacial phenomena.

Table 1
Homogeneous-equivalent atomic concentrations measured by XPS.

Peak	Atomic conc. %	Expected from PFDA
O 1s	5.8	6.3
C 1s	39.4	40.6
F 1s	54.8	53.1

The XPS survey spectra were used to determine the average homogeneous-equivalent atomic concentrations measured from 3 locations on the PFDA coated sample, the averages of which are reported in Table 1. An example survey spectrum is provided in the supplementary information (Fig. S.1 in the SI document). The measured atomic concentrations are in reasonable agreement with those that would be expected from a homogeneous layer of PFDA. No signal from the silicon substrate was observed, indicating that the coating layer is likely at least 10 nm thick, and free of pinholes or similar defects, or any that are present are below the detection limit for XPS (i.e. approx. <0.1% [57]).

Peak fitting of the carbon 1 s high-resolution spectra was performed in order to confirm the chemical composition of the coating layer - an example fit is shown in Fig. 2. Component positions, assignments, and their fraction of the C1s peak intensity are given in Table 2. A sum-Gaussian-Lorentzian line shape was used for the peaks, and the areas of peaks labelled C2 and C4 were constrained to be equal, as C2 was assumed to arise solely from the secondary shift caused by C4. Binding energies are reported referenced to the C-C component, which is assumed to lie at 285.0 eV. Several species are given multiple assignments, due to the presence of significant secondary chemical shifts and possible by-products of the plasma deposition method. The fractions of each species present are approximately consistent with the chemical structure of PFDA. As such intensities are determined assuming the material is homogeneous within the sampling depth, any form of ordering or layered structure will result in a skew in the observed intensities towards those components present closer to the surface; with this sample, in which the CF_3 end of the molecule is expected to form the uppermost surface, this should result in a higher proportion of the CF_3 species compared to CF_2, as is observed. The species

Table 2
Component assignments for carbon 1 s peak fit, and associated intensity fractions compared to that expected for PFDA. Binding energies are given relative to C—C, which is assumed to lie at 285.0 eV.

Component label	Binding Energy (eV)	Assignment	% of C 1s peak	Expected for PFDA
C1	285.0	C—C	14.1	15.4
C2	285.9	C—C secondary shift	10.1	7.7
C3	286.9	C—O/C—C secondary shift	7.0	7.7
C4	288.8	O=C—O/C—F	10.1	7.7
C5	291.2	CF_2	50.3	53.8
C6	293.4	CF_3	8.4	7.7

corresponding to a carboxyl group would however be expected to be localized beneath the surface, and therefore have a lower relative intensity compared to the 'homogeneous' expected intensity for PFDA. The slight increase in in this species is therefore unexpected and could indicate (i) fragmentation leading to the presence of C-F, (ii) additional carboxylic groups forming during the deposition process, and/or (iii) a deviation from a perfect alignment and orientation of PFDA molecules.

The wettability behavior of the sample is then exploited by carrying out contact angle measurements. In particular, 3 liquids with different polarity have been tested to estimate the droplet contact angles (Fig. 3 (a)) and to calculate the surface free energy of the sample. In order to highlight the role of PFDA coating, we carried out the CA measurements both on bare (untreated) and PFDA coated silicon. The water CA on the uncoated silicon sample is found equal to 47° ± 2°, whereas on the PFDA coating the CA corresponds to 144.8° ± 3.4, with a surface free energy of 2.05 mJ/m^2 (see Table 3) computed with the Owens-Wendt approach [14]. These first results demonstrate that the PFDA surface coating contributes to improve the hydrophobicity nature of silicon, reaching a total enhancement of 208% (see Fig. 3 (b)). It is worth noticing that the XPS analysis performed on the uncoated sample shows a presence of surface oxygen equal to 28% (see Fig. S.5 in the SI), which comes mainly from the oxidation of silicon and partially from other contamination. As pointed out by other authors in the literature, the oxidation of the most external layer confers the hydrophilic properties to the surface leading to a reduction of the water contact angle, from approximatively 80–90° (bare silicon without ambient agent exposure) to 30–40° (bare silicon under ambient agent exposure) [58,59–62]. However, also considering an uncontaminated silicon surface with a CA of 90°, our PFDA coating would guarantee an increase of hydrophobic properties equal roughly to 61% (see Fig. S.6 in the SI).

Although the previous experimental evidence may sufficiently complete the surface characterization of the PFDA coating, quantitative guidelines to orientate and focus the design are still missing. For a more comprehensive surface analysis and to give a better interpretation of the experimental results we then set-up a molecular modelling protocol, based on the XPS values illustrated in Table 2. Because of a slightly higher intensity of some carboxyl groups or C—F emerging from the XPS analysis compared to the expected PFDA values (see Table 2), we built four independent MD configurations by tuning the percentage of CF_x groups (see Fig. 4(a)) in the uppermost surface which is in contact with water.

Table 3
Contact angle measurements obtained with the experimental droplet method using three different liquids, namely: water, formamide, and methylene iodide.

Liquid	Contact Angle [°]
Water	144.8 ± 3.4
Formamide	136.8 ± 1.8
Methylene Iodide	126.8 ± 3.4

Thus, the PFDA-water interfaces have been arranged to show 0% (case (i) Fig. 5(a)), 60% (case (ii) Fig. 5(a)), 80% (case (iii) Fig. 5 (a)), and 100% (case (iv) Fig. 5 (a)) of CF_x groups. By applying the Free Energy Perturbation (FEP) approach (see Equation (5)), we calculated the work of adhesion, W_{sl} at PFDA-water interfaces and the resulting values are summarized in Fig. 5(b). An exemplifying case of the MD data post-processing is reported in the SI documentation. First, we notice that W_{sl} decreases with the enhancement of CF_x groups in contact with water. Specifically, considering the extreme configurations (i) and (iv), the W_{sl} goes from 52.9 ± 0.065 mJ/m^2 to 24.5 ± 0.065 mJ/m^2. It is worth noticing that the relative error on the interaction energy, U, due to thermal fluctuation is less than 5%. (see Fig. S.7 in SI document). The Young-Dupré model, described in the Eq. (6), is then used to obtain the contact angle values plotted in Fig. 5 (c). As expected, the contact angle ϑ increases with the CF_x groups, reaching the maximum value of 127.4° ± 1° for configuration (iv). These results already highlight the hydrophobic contribution induced by the ordered and structured alignment of the CF_x groups, confirming qualitatively the trend found in the droplet experiments (see Fig. 3(b)). Therefore, the polymer chemistry and orientation hold a dramatic effect on the wetting behavior. A further validation of the hydrophobicity given by the fluorine groups is shown in the layer of water molecules distributed within the first 0.5 nm at the PFDA interface (Fig. 4 (b)). The stronger adhesion of water in case of 0% surface CF_x results in a denser structure of molecules relating to the rest of PFDA orientations. It is worth noticing that such results are obtained for a smooth and planar surface only influenced by the chemical composition of the coating, in line with the hypothesis of the Young-Dupré equation.

A reliable and more quantitative comparison between the experimental contact angles and modelling results should be made for configurations (iii) and (iv) in Fig. 5(a), since they are in the closest match to the real chemical distribution of the PFDA (as shown in the XPS analysis). Within this window of configurations corresponding to contact angles between 120.2° ± 1° (iii) and 127.4° ± 1 (iv), we consider an average value of 123.8° ± 3.6° which shows a gap of 21° with respect to the experimental value (144.8° ± 3.4°). To explain this apparent mismatch, we recall the impact of topography in the surface wetting behavior. The molecular modelling, because of its intrinsic space-scale, is uniquely influenced by the surface atomic structure, therefore it is absolutely suitable to elucidate the chemistry contribution on the overall contact angle. On the other hand, the MD simulations are inadequate to reproduce the role of sample roughness and micro-surface patterning, that also play a significant role on the material hydrophobicity, thereby increasing the apparent contact angle. With this in mind, we can guess that the total contact angle enhancement obtained experimentally (208%) is affected by the surface chemistry for roughly the 78.5%, as suggested by the MD contact angle enhancement, and by topography for the remaining 21.5%, as shown in Fig. 3(b). In order to confirm and validate the enhancement of roughly 21° caused by the surface topography, we evaluated the surface roughness parameters obtained by the profilometric analy-

sis, in terms of arithmetic mean square and root mean square roughness, namely R_a = 0.025 ± 7·10^{-4} μm, and R_q = 0.0497 ± 4.2·10^{-3} μm, respectively. All the profilometric results are reported in Tables S.1–S.6 and Fig. S.8–S.10 in the SI document.

Coherent roughness values and related increments on apparent CA have been found in the literature on fluorinated materials. Coclite et al. [20] found an increment in advancing CA of PFDA of 26° with an improvement of R_q from 0.012 μm to 0.06 μm. Similarly, Christian et al. [22] used a heat treatment for the surface roughness reduction of PFDA from a R_q of 0.025 μm to 0.005 μm which corresponds to a reduction of apparent CA from approximately 140–120°. Shiu et al. [63] found a similar trend for the apparent CA of fluoropolymer depending on the increment of R_q. Thus, the roughness parameters of our PFDA coating can reasonably justify the topography enhancement of contact angle equal to 21°. In conclusion, with the integrated model suggested in this paper it is possible to quantify the chemical and the topographical contribution to the surface wettability, providing a more reliable and comprehensive understanding on the surface characterization.

5. Conclusions

In this article we have proposed a surface characterization platform to synergistically integrate experimental and modelling tools. The case study considered here is a (1H,1H,2H,2H)-Perfluorodecyl acrylate (PFDA) coated silicon surface fabricated with a semi-dynamic Dielectric Barrier Discharge (DBD) plasma technique. First, the experimental characterization of the surface, carried out with the XPS analysis and contact angle measurements has demonstrated a clear capability of PFDA coatings in the reduction of the surface free energy. In fact, the experimental results have reported an increase of water contact angle equal to 97.8°, passing from uncoated to PFDA coated silicon surface, thereby showing the evident hydrophobic nature of the sample. In order to provide a more comprehensive understanding of this interfacial behavior and guide the design, we used the XPS chemical quantitative results to build the atomistic model set-up and to perform molecular dynamics simulations. The Young contact angle obtained with the MD simulations and free energy perturbation approach quantitatively highlights the contribution of surface chemistry and consequentially of surface texture on the experimental surface characterization. On one hand, MD simulations show that the chemical coating of PFDA on silicon surface is able to bring the contact angle (CA) to roughly 123.8° ± 3.6°, which confirms low affinity of PFDA with water, making the silicon surface more hydrophobic (considering a flat surface). On the other hand, the experimental profilometric parameters demonstrate to fill the gap, contributing to enhance the contact angle from 123.8° ± 3.6° to 144.8° ± 3.4°. Indeed, the latter increment follows similar trends reported by previous experimental results in the same range of root mean square roughness on fluorinated surface [19,20,22]. Therefore, regarding our case study, the surface chemistry accounts for roughly 78.5% of the total increase of the contact angle; further effects like the physical roughness and patterning contribute to the remaining 21.5%.

In conclusion, our modeling and experimental integrated protocol can decouple the chemistry and physical contribution on the apparent contact angle of a hydrophobic surface. In addition, the approach suggested in this paper clarifies a deeper understanding about the surface characterization and represents a good protocol for the first steps towards an optimized surface design. It is worth noticing that such a protocol does not complete the tailored design of super hydrophobic surfaces, which instead requires the development of an optimized surface topology. An interesting perspective of this work may certainly include a sensitivity analysis of thermodynamics input parameters, like temperature or pressure, on the resulting surface wetting properties. In particular, a thorough analysis of the uncertainty quantification (UQ) [64] may definitely address a more precise material design in a wide range of operating conditions.

CRediT authorship contribution statement

Annalisa Cardellini: Conceptualization, Methodology, Data curation, Formal analysis, Visualization, Investigation, Writing - original draft. **Francesco Maria Bellussi:** Software, Data curation, Investigation, Formal analysis, Visualization, Writing - original draft. **Edoardo Rossi:** Validation, Investigation, Visualization. **Lorenzo Chiavarini:** Software, Data curation, Investigation, Formal analysis, Visualization. **Claude Becker:** Methodology, Investigation, Resources, Funding acquisition. **David Cant:** Methodology, Investigation, Data curation, Investigation, Formal analysis, Visualization. **Pietro Asinari:** Conceptualization, Supervision, Writing - review & editing, Funding acquisition. **Marco Sebastiani:** Conceptualization, Resources, Supervision, Writing - review & editing, Funding acquisition.

Declaration of Competing Interest

The authors declare that they have no known competing financial interests or personal relationships that could have appeared to influence the work reported in this paper.

Acknowledgements

The authors gratefully acknowledge financial support from the European Commission, European project Oyster, www.oyster-project.eu, grant agreement n. 760827. A.C., L.C., F.M.B, and P.A. thank the CINECA (Iscra C and Iscra B projects), and Politecnico di Torino's High Performance Computing Initiative (http://hpc.polito.it/) for the availability of computing resources and support. Contact angle measurements were carried out at the "Inter-Departmental Laboratory of Electron Microscopy" (LIME), Università degli studi Roma TRE (**http://www.lime.uniroma3.it**).

Data availability

The Molecular Dynamics raw and processed data required to reproduce these findings are available in the Supporting Information documentation. Some of the experimental raw data required to reproduce these findings cannot be shared at this time due to technical limitations.

Appendix A. Supplementary material

Supplementary data to this article can be found online at https://doi.org/10.1016/j.matdes.2021.109902.

References

[1] D. Wang, Q. Sun, M.J. Hokkanen, C. Zhang, F.Y. Lin, Q. Liu, S.P. Zhu, T. Zhou, Q. Chang, B. He, Q. Zhou, L. Chen, Z. Wang, R.H.A. Ras, X. Deng, Design of robust superhydrophobic surfaces, Nature 582 (2020) 55–59, https://doi.org/10.1038/s41586-020-2331-8.

[2] S.S. Latthe, R.S. Sutar, V.S. Kodag, A.K. Bhosale, A.M. Kumar, K. Kumar Sadasivuni, R. Xing, S. Liu, Self – cleaning superhydrophobic coatings: Potential industrial applications, Prog. Org. Coat. 128 (2019) 52–58, https://doi.org/10.1016/j.porgcoat.2018.12.008.

[3] S. Rasouli, N. Rezaei, H. Hamedi, S. Zendehboudi, X. Duan, Superhydrophobic and superoleophilic membranes for oil-water separation application: A comprehensive review, Mater. Des. 204 (2021), https://doi.org/10.1016/j.matdes.2021.109599 109599.

[4] G.G. Jang, D.B. Smith, G. Polizos, L. Collins, J.K. Keum, D.F. Lee, Transparent superhydrophilic and superhydrophobic nanoparticle textured coatings: Comparative study of anti-soiling performance, Nanoscale Adv. 1 (2019) 1249–1260, https://doi.org/10.1039/c8na00349a.
[5] Y. Zhu, F. Yang, Z. Guo, Bioinspired surfaces with special micro-structures and wettability for drag reduction: Which surface design will be a better choice?, Nanoscale 13 (2021) 3463–3482, https://doi.org/10.1039/d0nr07664c.
[6] L. Mazzola, M. Sebastiani, E.E. Bemporad, F.F. Carassiti, An innovative non-contact method to determine surface free energy on micro-areas, J. Adhes. Sci. Technol. 26 (2012) 131–150, https://doi.org/10.1163/016942411X569354.
[7] E.M. Rossi, P.S. Phani, R. Guillemet, J. Cholet, D. Jussey, W.C. Oliver, M. Sebastiani, A novel nanoindentation protocol to characterize surface free energy of superhydrophobic nanopatterned materials, J. Mater. Res. (2021) 1–14, https://doi.org/10.1557/s43578-021-00127-3.
[8] B.V. Derjaguin, V.M. Muller, Y.P. Toporov, Effect of contact deformation on the adhesion of elastic solids, J. Colloid Interface Sci. 53 (1975) 314–326.
[9] Z. Peng, J. Song, Y. Gao, J. Liu, C. Lee, G. Chen, Z. Wang, J. Chen, M.K.H. Leung, A fluorinated polymer sponge with superhydrophobicity for high-performance biomechanical energy harvesting, Nano Energy 85 (2021), https://doi.org/10.1016/j.nanoen.2021.106021 106021.
[10] X. Li, T. Shi, B. Li, X. Chen, C. Zhang, Z. Guo, Q. Zhang, Subtractive manufacturing of stable hierarchical micro-nano structures on AA5052 sheet with enhanced water repellence and durable corrosion resistance, Mater. Des. 183 (2019), https://doi.org/10.1016/j.matdes.2019.108152 108152.
[11] N. Wang, L. Tang, W. Tong, D. Xiong, Fabrication of robust and scalable superhydrophobic surfaces and investigation of their anti-icing properties, Mater. Des. 156 (2018) 320–328, https://doi.org/10.1016/j.matdes.2018.06.053.
[12] J. Hasan, S. Jain, R. Padmarajan, S. Purighalla, V.K. Sambandamurthy, K. Chatterjee, Multi-scale surface topography to minimize adherence and viability of nosocomial drug-resistant bacteria, Mater. Des. 140 (2018) 332–344, https://doi.org/10.1016/j.matdes.2017.11.074.
[13] M.D. Wellcome, An essay on roses, An Essay Roses (2011), https://doi.org/10.5962/bhl.title.36978.
[14] D.K. Owens, R.C. Wendt, Estimation of the surface free energy of polymers, J. Appl. Polym. Sci. (1969), https://doi.org/10.1002/app.1969.070130815.
[15] R.N. Wenzel, Resistance of solid surfaces to wetting by water, Ind. Eng. Chem. 28 (1936) 988–994, https://doi.org/10.1021/ie50320a024.
[16] B.D. Cassie, Of porous surfaces, (1944) 546–551.
[17] E. Bormashenko, General equation describing wetting of rough surfaces, J. Colloid Interface Sci. 360 (2011) 317–319, https://doi.org/10.1016/j.jcis.2011.04.051.
[18] X. Zeng, Y. Ma, Y. Wang, Enhancing the low surface energy properties of polymer films with a dangling shell of fluorinated block-copolymer, Appl. Surf. Sci. (2015), https://doi.org/10.1016/j.apsusc.2015.02.134.
[19] M. Karaman, T. Uçar, Enhanced mechanical properties of low-surface energy thin films by simultaneous plasma polymerization of fluorine and epoxy containing polymers, Appl. Surf. Sci. (2016), https://doi.org/10.1016/j.apsusc.2015.11.254.
[20] A.M. Coclite, Y. Shi, K.K. Gleason, Grafted crystalline poly-perfluoroacrylate structures for superhydrophobic and oleophobic functional coatings, Adv. Mater. 24 (2012) 4534–4539, https://doi.org/10.1002/adma.201200682.
[21] S. Giljean, M. Bigerelle, K. Anselme, H. Haidara, New insights on contact angle/roughness dependence on high surface energy materials, Appl. Surf. Sci. 257 (2011) 9631–9638, https://doi.org/10.1016/j.apsusc.2011.06.088.
[22] P. Christian, A.M. Coclite, Vapor-phase-synthesized fluoroacrylate polymer thin films: Thermal stability and structural properties, Beilstein J. Nanotechnol. 8 (2017) 933–942, https://doi.org/10.3762/bjnano.8.95.
[23] P. Rytlewski, M. Zenkiewicz, Laser-induced surface modification of polystyrene, Appl. Surf. Sci. 256 (2009) 857–861, https://doi.org/10.1016/j.apsusc.2009.08.075.
[24] L. Ponsonnet, K. Reybier, N. Jaffrezic, V. Comte, C. Lagneau, M. Lissac, C. Martelet, Relationship between surface properties (roughness, wettability) of titanium and titanium alloys and cell behaviour, Mater. Sci. Eng. C 23 (2003) 551–560, https://doi.org/10.1016/S0928-4931(03)00033-X.
[25] P. De Angelis, A. Cardellini, P. Asinari, Exploring the free energy landscape to predict the surfactant adsorption isotherm at the nanoparticle-water interface, ACS Cent. Sci. 5 (2019) 1804–1812, https://doi.org/10.1021/acscentsci.9b00773.
[26] S. Salassi, A. Cardellini, P. Asinari, R. Ferrando, G. Rossi, Water dynamics affects thermal transport at the surface of hydrophobic and hydrophilic irradiated nanoparticles, Nanoscale Adv. 2 (2020) 3181–3190, https://doi.org/10.1039/d0na00094a.
[27] A. Cardellini, M. Alberghini, A. Govind Rajan, R.P. Misra, D. Blankschtein, P. Asinari, Multi-scale approach for modeling stability, aggregation, and network formation of nanoparticles suspended in aqueous solutions, Nanoscale 11 (2019) 3925–3932, https://doi.org/10.1039/c8nr08782b.
[28] A. Cardellini, M. Fasano, E. Chiavazzo, P. Asinari, Interfacial water thickness at inorganic nanoconstructs and biomolecules: Size matters, Phys. Lett. A 380 (2016) 1735–1740, https://doi.org/10.1016/J.PHYSLETA.2016.03.015.
[29] V. Sresht, A. Govind Rajan, E. Bordes, M.S. Strano, A.A.H. Pádua, D. Blankschtein, Quantitative Modeling of MoS2-Solvent Interfaces: Predicting Contact Angles and Exfoliation Performance using Molecular Dynamics, J. Phys. Chem. C (2017), https://doi.org/10.1021/acs.jpcc.7b00484.
[30] R.P. Misra, D. Blankschtein, Insights on the Role of Many-Body Polarization Effects in the Wetting of Graphitic Surfaces by Water, J. Phys. Chem. C (2017), https://doi.org/10.1021/acs.jpcc.7b08891.
[31] H. Jiang, F. Müller-Plathe, A.Z. Panagiotopoulos, Contact angles from Young's equation in molecular dynamics simulations, J. Chem. Phys. (2017), https://doi.org/10.1063/1.4994088.
[32] J.A. Barker, D. Henderson, Perturbation theory and equation of state for fluids. II. A successful theory of liquids, J. Chem. Phys. (1967), https://doi.org/10.1063/1.1701689.
[33] F. Leroy, S. Liu, J. Zhang, Parametrizing Nonbonded Interactions from Wetting Experiments via the Work of Adhesion: Example of Water on Graphene Surfaces, J. Phys. Chem. C (2015), https://doi.org/10.1021/acs.jpcc.5b10267.
[34] H. Jiang, A.J. Patel, Recent advances in estimating contact angles using molecular simulations and enhanced sampling methods, Curr. Opin. Chem. Eng. (2019), https://doi.org/10.1016/j.coche.2019.03.012.
[35] M. Ernstsson, T.D. Wärnheim, Surface analytical techniques applied to cleaning processes, Handb. Cleaning/Decontam. Surf. 2 (2007) 747–789, https://doi.org/10.1016/B978-044451664-0/50023-1.
[36] J. Petersen, C. Becker, T. Fouquet, F. Addiego, V. Toniazzo, A. Dinia, D. Ruch, Nano-ordered thin films achieved by soft atmospheric plasma polymerization, RSC Adv. 3 (2013) 4416–4424, https://doi.org/10.1039/c2ra21833j.
[37] G. Mertz, T. Fouquet, C. Becker, F. Ziarelli, D. Ruch, A methacrylic anhydride difunctional precursor to produce a hydrolysis-sensitive coating by aerosol-assisted atmospheric plasma process, Plasma Process. Polym. 11 (2014) 728–733, https://doi.org/10.1002/ppap.201400050.
[38] T. Fouquet, G. Mertz, M. Delmée, L. Fetzer, C. Becker, Thermal Analysis Goes with Mass Spectrometry to Evaluate the Molecular Weight of a Fluorinated Plasma Polymer, Plasma Process. Polym. 12 (2015) 980–990, https://doi.org/10.1002/ppap.201500038.
[39] M.P. Seah, XPS reference procedure for the accurate intensity calibration of electron spectrometers— results of a BCR intercomparison co-sponsored by the VAMAS SCA TWA, Surf. Interface Anal. (1993), https://doi.org/10.1002/sia.740200309.
[40] M.P. Seah, Background subtraction: I. General behaviour of Tougaard-style backgrounds in AES and XPS, Surf. Sci. (1999), https://doi.org/10.1016/S0039-6028(98)00852-8.
[41] L. Černe, B. Simončič, Influence of Repellent Finishing on the Surface Free Energy of Cellulosic Textile Substrates, Text. Res. J. (2004), https://doi.org/10.1177/004051750407400509.
[42] A. Relini, S. Sottini, S. Zuccotti, M. Bolognesi, A. Gliozzi, R. Rolandi, Measurement of the surface free energy of streptavidin crystals by atomic force microscopy, Langmuir (2003), https://doi.org/10.1021/la026515g.
[43] M. Zenkiewicz, Comparative study on the surface free energy of a solid calculated by different methods, Polym. Test. (2007), https://doi.org/10.1016/j.polymertesting.2006.08.005.
[44] A. Rudawska, E. Jacniacka, Analysis for determining surface free energy uncertainty by the Owen-Wendt method, Int. J. Adhes. Adhes. (2009), https://doi.org/10.1016/j.ijadhadh.2008.09.008.
[45] E. McCafferty, Acid-base effects in polymer adhesion at metal surfaces, J. Adhes. Sci. Technol. (2002), https://doi.org/10.1163/156856102317295478.
[46] C. Della Volpe, S. Siboni, Some reflections on acid-base solid surface free energy theories, J. Colloid Interface Sci. (1997), https://doi.org/10.1006/jcis.1997.5124.
[47] K. Mittal, Advances in Contact Angle, Wettability and Adhesion, John Wiley & Sons Inc, Hoboken, NJ, USA, 2015. 10.1002/9781119117018.
[48] N.M. O'Boyle, M. Banck, C.A. James, C. Morley, T. Vandermeersch, G.R. Hutchison, Open Babel: An Open chemical toolbox, J. Cheminform. (2011), https://doi.org/10.1186/1758-2946-3-33.
[49] C. Kutzner, S. Páll, M. Fechner, A. Esztermann, B.L. de Groot, H. Grubmüller, More bang for your buck: Improved use of GPU nodes for GROMACS 2018, J. Comput. Chem. (2019), https://doi.org/10.1002/jcc.26011.
[50] S.W.I. Siu, K. Pluhackova, R.A. Böckmann, Optimization of the OPLS-AA force field for long hydrocarbons, J. Chem. Theory Comput. (2012), https://doi.org/10.1021/ct200908r.
[51] D. Shivakumar, J. Williams, Y. Wu, W. Damm, J. Shelley, W. Sherman, Prediction of absolute solvation free energies using molecular dynamics free energy perturbation and the opls force field, J. Chem. Theory Comput. 6 (2010) 1509–1519, https://doi.org/10.1021/ct900587b.
[52] C. Vega, E. De Miguel, Surface tension of the most popular models of water by using the test-area simulation method, J. Chem. Phys. (2007), https://doi.org/10.1063/1.2715577.
[53] H. Chávez Thielemann, A. Cardellini, M. Fasano, L. Bergamasco, M. Alberghini, G. Ciorra, E. Chiavazzo, P. Asinari, From GROMACS to LAMMPS: GRO2LAM: A converter for molecular dynamics software, J. Mol. Model. (2019), https://doi.org/10.1007/s00894-019-4011-x.
[54] S. Plimpton, Fast parallel algorithms for short-range molecular dynamics, J. Comput. Phys. (1995), https://doi.org/10.1006/jcph.1995.1039.
[55] S. Nosé, A unified formulation of the constant temperature molecular dynamics methods, J. Chem. Phys. (1984), https://doi.org/10.1063/1.447334.
[56] N.K. Adam, Use of the Term 'Young's Equation' for Contact Angles, Nature. 180 (1957) 809–810, https://doi.org/10.1038/180809a0.
[57] A.G. Shard, Detection limits in XPS for more than 6000 binary systems using Al and Mg Kα X-rays, Surf. Interface Anal. (2014), https://doi.org/10.1002/sia.5406.

[58] C. Xiao, C. Chen, Y. Yao, H. Liu, L. Chen, L. Qian, S.H. Kim, Nanoasperity Adhesion of the Silicon Surface in Humid Air: The Roles of Surface Chemistry and Oxidized Layer Structures, Langmuir 36 (2020) 5483–5491, https://doi.org/10.1021/acs.langmuir.0c00205.
[59] L. Chen, D. Ngo, J. Luo, Y. Gong, C. Xiao, X. He, B. Yu, L. Qian, S.H. Kim, Dependence of water adsorption on the surface structure of silicon wafers aged under different environmental conditions, Phys. Chem. Chem. Phys. 21 (2019) 26041–26048, https://doi.org/10.1039/c9cp04776j.
[60] M. Barisik, A. Beskok, Wetting characterisation of silicon (1,0,0) surface, Mol. Simul. 39 (2013) 700–709, https://doi.org/10.1080/08927022.2012.758854.
[61] J. Chai, S. Liu, X. Yang, Molecular dynamics simulation of wetting on modified amorphous silica surface, Appl. Surf. Sci. 255 (2009) 9078–9084, https://doi.org/10.1016/j.apsusc.2009.06.109.
[62] H.A. Zambrano, J.H. Walther, R.L. Jaffe, Molecular dynamics simulations of water on a hydrophilic silica surface at high air pressures, J. Mol. Liq. 198 (2014) 107–113, https://doi.org/10.1016/j.molliq.2014.06.003.
[63] J.Y. Shiu, P. Chen, Addressable protein patterning via switchable superhydrophobic microarrays, Adv. Funct. Mater. 17 (2007) 2680–2686, https://doi.org/10.1002/adfm.200700122.
[64] N. Vu-Bac, T. Lahmer, X. Zhuang, T. Nguyen-Thoi, T. Rabczuk, A software framework for probabilistic sensitivity analysis for computationally expensive models, Adv. Eng. Softw. 100 (2016) 19–31, https://doi.org/10.1016/j.advengsoft.2016.06.005.
[65] V. Ballenegger, A. Arnold, J.J. Cerdà, Simulations of non-neutral slab systems with long-range electrostatic interactions in two-dimensional periodic boundary conditions, J. Chem. Phys. 131 (9) (2009).